Industrial Crops and Products, Volume 204, Part B, Article number 117307
DOI:10.1016/j.indcrop.2023.117307

Development of Reduced Graphene Oxide (rGO) reinforced Poly(Lactic) Acid/ Cellulose nanocrystal composite through Melt Mixing: Effect of nanofiller on Thermal, Structural, Biodegradation and Antibacterial properties

Kartikey Verma[a,b*], Salim H. Siddiki[c], Chandan Kumar Maity[c], Raghvendra Kumar Mishra[d],& Md Moniruzzaman[e**]

[a]*Department of Chemical Engineering, Indian Institute of Technology Kanpur, Kalyanpur, Kanpur, Uttar Pradesh 208016, India*

[b]*Allements Energy Solutions Pvt. Ltd, Lucknow, Uttar Pradesh 226021, India*

[c] *Department of Chemistry and Chemical Biology, IIT (ISM) Dhanbad, 826004, Dhanbad,India*

[d]*Cranfield University, Bedford MK43, UK*

[e]*Department of Chemical and Biological Engineering, Gachon University, 1342 Seongnam-daero, Seongnam-si, Gyeonggi-do 13120, Republic of Korea*

*Corresponding Author: *Kartikey Verma; Email id: vrmakrtk@gmail.com
:**Md Moniruzzaman; Email id: mani57chem@gachon.ac.kr

Abstract: The intent of this research work was to synthesised a synthetic polymer that is biodegradable, bioresorbable, and biocompatible, while also exhibiting favorable thermal characteristics. The present study reports the successful fabrication of bionanocomposites by incorporating Cellulose nanocrystals (CNCs) and Reduced graphene oxide (rGO) into host matrix (PLA) using the melt-mixing technique. Various weight percentages (wt.%) of rGO were employed in the process and various characterization techniques, including BET analysis, XRD, FTIR and field emission scanning electron microscopy (FE-SEM) were used to verify the efficient fabrication of a number of nanoformulations and nanofiller's effect. Introduction of CNC and rGO in PLA matrix increases the surface area as well as porosity of the composites, established by BET analysis. DSC results indicate that the

assimilation of rGO into the polymer matrix improved thermal stability of the composite material and leads to boost in the degree of crystallinity which was supported by XRD analysis. TGA results found no noticeable change in glass transition temprature (Tg) due to the addition of Nanofiller (rGO). The wettability analysis was done by contact angle measurement to determine the hydrophilicity of the composite and it is shown that with the increasing amount of rGO, hydrophilicity increases and contact angle reaches to 69^{o} for 0.75wt% of rGO in composite in comparision to 100^{o} Neat PLA . The rGO/CNC/PLA nanocomposites exhibit a unique antibacterial effectiveness against both the S. aureus (Gram-positive) and E. coli (Gram-negative) bacterial strains. The highest antimicrobial activity was obtained in the nanocomposite tested against S. aureus. Biodegradation through Lysozyme in PBS solution shows promising result after incorporation of nanofillers. Hence, the nanocomposite manufactured through melt mixing process has promising uses in the biomedical and food packaging industries.

Keywords: Poly Lactic Acid, Reduced graphene oxide, Surface Area, wettability, Biodegradibility

1. Introduction:

Trends in composite technology away from conventional materials are being driven by the increasing pressure on manufacturers from waste management rules and new environmental policies, customer demand, and rising oil prices. There is a growing inclination to substitute conventional plastics with green composite materials in consumer goods, with the aim of enhancing efficacy, while simultaneously mitigating costs and weight. [1,2] Lactic acid is one such resource; when polymerized into polylactic acid (PLA), it creates a renewable plastic material that could replace petroleum-based polymers in the long run. PLA possesses several benefits such as its inherent biodegradability and adaptability, as well as its sourcing from renewable natural resources. The production of PLA entails a significantly lower energy consumption of about 65% compared to the conventional plastics. Additionally, it generates a reduced amount of greenhouse gases by approximately 68%. Furthermore, in the event of incineration, PLA releases less toxic fumes than the majority of petroleum-based alternatives [3-5]. Although PLA offers numerous benefits, it is imperative to acknowledge its drawbacks in order to facilitate its substitution for non-renewable plastics in commonplace uses. A significant drawback associated with PLA is its suboptimal performance when utilized as a barrier material [6]. Another drawback pertains to its inadequate durability [5]. Upon exposure to humidity, the polymer undergoes hydrolysis reactions due to the permeation of water molecules, ultimately advances to the degradation of its crystalline structure. To tackle these concerns, researchers are endeavoring to alter PLA by incorporating nanofillers that have the potential to curtail vapor transmission across the composite material, thereby potentially decelerating degradation that is based on hydrolysiS [7-9]. Inert nanomaterials such as graphene, CNT(carbon nanotubes), and nanoclays have the potential to serve as nanofillers in polymer matrices, resulting in the fabrication of nanocomposites that exhibit enhanced physicochemical

properties when compared to basic polymers and conventional composites.[10-12] The mechanical characteristics of polymer nanocomposites are contingent upon two factors that pose a challenge to achieve concurrently. Two critical factors, affetcting the performance of nanocomposites are the dispersion of the nanofiller in a hydrophobic polymer matrix & the existence of attractive interfacial interactions with the nanofillers and matrices [13,14]. The nanofillers' high surface energy and propensity for accumulation in hydrophobic polymer matrices are responsible for this. Hence, in order to surmount this challenge, it is imperative to engage in surface modification of nanofillers to attain a potent nanocomposite impact with minimal incorporation into the polymer [15].

Depending on the sources from which cellulose is derived, Cellulose nanocrystals (CNC) are commonly characterized as inflexible, rod-like, and composed of single-crystalline cellulose domains with diameter 1-100 nm & 10-100 nm length [16]. Cellulose nanocrystals (CNC) possess a crystalline structure, exhibit a significantly good aspect ratio (near 70), and possess a substantial surface area (approximately 150 m^2/g). Cellulose nanocrystals can be generated through the process of acid hydrolysis applied to diverse natural cellulose fibers, including cellulose fibers sourced from lignocellulosic materials,cotton, and tunicate derived from marine animals [16]. Cellulose nanocrystals exhibit superior mechanical characteristics in comparison to the majority of the frequently employed reinforcement agents. Their extraordinary unique properties, including as biocompatibility and biodegradability , low density and high stiffness, are to their favor [17].

Graphene is a 2-D material composed of carbon atoms that are hybridized with sp^2 orbitals. Graphene exhibits several distinctive characteristics that distinguish it from other carbon allotropes [18-19]. These include a notably large surface area (2600 m^2/g), exceptional electrical conductivity, remarkable flexibility, excellent mechanical strength,

and efficient electron transport [20-21]. Additionally, graphene displays a high thermal conductivity of 500W/mK and is sustainable for the environment. [22-24] Reduced Graphene oxide (rGO), which consists mainly of sp^2 hybridized 2D carbon layers that are only a few atoms thick and contain some oxygen functional groups at the edges, is considered a leading nanofiller due to its remarkable physical and chemical characteristics, including exceptional mechanical, electrical, and thermal properties [25-29]. Extensive research has been conducted on this topic across multiple disciplines within the realms of technological innovation and science. Wang et al. in their research work have studied the outcome of rGO incorporation on both the thermal & mechanical characteristics of blends comprising of PBS (poly butylene succinate) and PLA [30]. The findings indicated a heightened level of compatibility between PLA and PBS, leading to improved thermal characteristics and higher storage modulus. Moreover , the homogeneous distribution of reduced graphene oxide (rGO) within PLA/ PBS/rGO resulted in an enhancement of their tensile and impact properties.

This study utilizes a meltmixing technique to create CNC/rGO/PLA nanocomposites with the intent of exploring their potential utility in the biomedical and packaging industries [31]. The present investigation involved the synthesis of CNC via acid hydrolysis, followed by the incorporation of rGO as an additional nanofiller into the CNC/PLA nanocomposite. The purpose of this work was to investigate the enzymatic degradation of PLA tweaked with CNC because of the relevance of the biodegradation of PLA reinforced with cellulose nanocrystal fillers and the inconsistency of existing data. Reduced graphene oxide was used to modify the thermal properties of the resulting nanocomposites. The concentration of CNC was kept 1 wt% because previously few have reported best results with this CNC loading in PLA matrix [32]. The weight percentage of rGO was varied from 0.25-0.75 wt%. Using FESEM, we analyzed how well

CNC and rGO were dispersed in a polymer matrix. The nanocomposite's structural properties and attached functional groups were analyzed using FTIR and XRD characterizations. In addition to the primary investigation, supplementary analyses were conducted, including DSC, contact angle measurement, TGA and BET analysis. Composites containing varying amounts of rGO were analyzed to determine the composite's antibacterial performance. This investigation evaluated the antibacterial activity of nanocomposites against Gram-positive Staphylococcus aureus (S.aureus) and Gram-negative Escherichia coli (E.coli) bacteria.

2. Experimental Section

2.1 Materials and methods:

The chemical reagents utilized in the synthesis, reduction, and purification of rGO were purchased from Sigma Aldrich (India) and had purity levels exceeding 99.9%. These reagents include hydrochloric acid (HCl, 10%), graphite powder, sulfuric acid, potassium permanganate ($KMnO_4$), orthophosphoric acid, selenium powder (particle size: 100 mesh), and hydrogen peroxide (H_2O_2, 30%). Microcrystalline Cellulose (MCC) was ordered from Sigma Aldrich (India) with purity >99.9%. Poly Lactic Acid (PLA 4044D) was procured from Natur-Tec , India.

2.1.1 Synthesis of Cellulose Nanocrystals:

Synthesis of CNCs was carried out by mimicking the procedure described by Cranston and Gray [33]. First, a suspension of 15 g of MCC powder in 150 mL of deionized water was made. Sulfuric acid (64-65 (wt/wt%) of 225 mL was dropwise added to perform the hydrolysis at 45^{o}C on a magnetic stirrer. The agitation was sustained for a duration of three hours. The suspension was subsequently added with deionized cold water (4^{o}C) at a ratio of 1:10 after the hydrolysis process was complete. Following a period of 3-4 hours, the

suspension underwent centrifugation at a rate of 5000 rotations per minute for a duration of 15 minutes, with the aim of eliminating the acid and increasing the concentration of the cellulose suspension. The resulting precipitate was based on a rinsing process & subsequently underwent centrifugation at a rate of 5000 revolutions per minute, utilizing deionized water until a state of neutral pH was achieved. For the next four days, the precipitate was dialyzed against deionized water via a cellulose dialysis membrane to keep the pH constant at 7. The nanocrystals were synthesized via a sequence of ultrasonic treatments at 65% output for a duration of 20 minutes in an ice-cold bath utilizing a tip sonicator. The cellulose suspension obtained had a weight percentage of approximately 1% and a yield of approximately 20%. Subsequently, the CNC suspension underwent lyophilization.Then cellulose nanocrystals (CNC) were freeze-dried and subsequently refrigerated for future utilization.

2.1.2 Synthesis of rGO by using Se powder:

For the production of rGO, we have used the same procedure , published recently by using Se powder [34]. In short, 9:1 (720 mL) mixture of concentrated H_2SO_4 and H_3PO_4 was used to oxidize graphite powder (6.0 g, 1 wt %), and this was followed by the gradual addition of $KMnO_4$ powder (36 g, 6 wt %). A small exothermic phase (about 40 °C) occurs during the addition of $KMnO_4$. Following the addition of KMnO4, the mixture was subjected to constant stirring at a temperature of 60 °C for a duration of 15 hours.. Upon cooling of the reaction mixture to ambient temperature, it was subsequently transferred into an ice bath (500 mL) and 6 mL of 30% H_2O_2 was added very slowly, drop by drop, in a dark room. To clean up, we washed the reaction mixture few times with deionized water until the pH was neutralized (about 6.5 slightly acidic), centrifuged it at 3000 rpm for 2 hours, and then drained the supernatant. Subsequently, the residual substance underwent a series of washes using 400 mL of deionized water, followed by 400 mL of 30% hydrochloric acid, and

finally 400 mL of ethanol. Ultimately, the resolution was subjected to filtration through a polytetrafluoroethylene (PTFE) membrane. After obtaining the product on the PTFE membrane, which consisted of approximately 10 g of graphene oxide, it underwent a drying process under vacuum conditions for 48 hours at 45°C. We employed 0.3 g of Se powder to convert 3 g of totally exfoliated GO nano sheets into rGO. The Se powder and GO were meticulously mixed using a mortar and pestle under dry conditions. The resulting mixture was subsequently enclosed within a quartz tube, under an inert atmosphere. The tube was heated for 5 minutes in a furnace set to 360 degrees Celsius. The final product was subjected to a thorough washing process using distilled water in order to remove any impurities.

2.1.3Synthesis of PLA/CNC /rGO nanocomposites

The production of PLA/CNC/rGO nanocomposites was carried out using a melt-mixing technique. PLA, rGO and CNC were subjected to a drying process at 80°C for a duration of 10 hours ahead of compounding. The production of the composite materials, consisting of a neat PLA , CNC and rGO, was accomplished through the process of melt compounding. This was achieved by utilizing a twin-screw extruder (manufactured by Fly Tech Engineering, located in Chennai, India) that operated at a shear rotation of 30 revolutions per minute and at 180°C for 10 minutes. The process of melting was observed in the granules, leading to their transformation into a semisolid state. Following this, the addition of 1 wt% of CNC and 0.25-0.75wt% of rGO was gradually introduced into the mixture, resulting in the formation of distinct nanocomposites. Compression molding was performed after removing the semisolid nanocomposite from the internal mixture machine, where it had been mixed for 5 minutes. This involved utilizing a hot press at 180°C, whereby an increasing force was applied over a period of approximately 5 minutes until a thickness of 1 mm was achieved (as per ASTM standard for polymeric materials). The cast samples

were allowed to be brought to room temperature in ambient air. The PLA, CNC and rGO composition is given in Table 1.

Table 1: Code and composition of different nanocomposites

Sample Code	**PLA** Percentage(wt %)	**CNC** Percentage(wt %)	**rGO** Percentage(wt %)	**Processing Condition**
Sample 1	100	-	-	Rpm-30 Temp- 180ºC
Sample 2	99	1	-	Same
Sample 3	98.75	1	0.25	Same
Sample 4	98.50	1	0.50	Same
Sample 5	98.25	1	0.75	Same

2.2 Characterization:

2.2.1 FTIR : Reflectance attenuation ATR-FTIR was done on extruded film samples by using a Bruker Tensor 27 FT-IR Spectrometer with a wavelength resolution of 4 cm^{-1}, 64 scans in the 4000-500 cm^{-1} range were used to get each spectra. Samples with comparable thickness were subjected to a 24-hour drying process in an oven set at 60 ºC before undergoing testing. To ensure comparability across all spectra, the sample thickness was consistently maintained at a uniform level. The rationale behind this approach stems from the fact that the intensity of a peak in the FTIR absorption spectrum is impacted by the distance traversed by the infrared radiation, which is intrinsically linked to the thickness of the sample.

2.2.2 X-ray diffraction (XRD) : X-ray diffraction (XRD) is a widely employed analytical tool for investigating the crystallographic properties of materials. The investigation of the

crystal structure of films was conducted utilizing a Panalytical XPert Advance powder X-ray diffractometer with a Cu Ka target (λ = 0.15404 nm). The angle range of the investigation was 5°–70°, with 1°/min scan rate.

2.2.3 Field Emission Scanning electron microscopy (FESEM): The surface morphology of the films was assessed through the utilization of FESEM Tescan MIRA3, operating at an acceleration voltage of 10 KV and 20 mm working distance. After cutting the samples into little pieces, the pieces were then glued on top of the conductive carbon tape. The samples were subjected to a treatment in which they were submerged in liquid nitrogen and then coated with a layer of gold for a period of 90 seconds, using a sputter-coating equipment.

2.2.4 BET Analysis: The determination of the specific surface area was conducted using the Brunauer, Emmet, and Teller method, commonly referred to as BET. The Quanta chrome Autosorb 1C analyzer was utilized to conduct measurements, with nitrogen serving as the sorption agent and an adsorption isotherm at a temperature of 77 K. About 2 g of each sample was weighed and utilized in each experiment. Preceding the analysis, the samples were taken to a drying process at 110 °C for a duration of 24 hours, followed by degassing at ambient temperature.

2.2.5 Thermogravimetric Analysis : The thermogravimetric analysis (TGA) was used to examine the characteristics of thermal degradation for all of the extruded sample. The study involved conducting experiments on a TA Instruments (DSC SDT Q600 Thermogravimetric Analyzer) in liquid nitrogen, from 25 to 600 °C. The heating rate employed during the experiments was 10 °C/min.

2.2.6 Differential Scanning Calorimetry: The thermal characteristics were additionally evaluated through the utilization of differential scanning calorimetry (DSC). The experimental setup involved the utilization of a TA Instruments (DSC Q25) apparatus with

a N_2 purge rate of 50 mL/min. Equilibrated in the DSC at 10 °C, samples weighing 10 mg were put into aluminum pans. Subsequently, the specimens underwent a heating process at a rate of 10°C/min, culminating at a maximum 180 °C, following a cooling process at the same rate, until reaching the initial temperature of 10 °C. All samples underwent three such cycles of temperature changes between 10 and 180 °C and returned to 10.

2.2.7 Antibacterial Assesment : The antibacterial efficacy of various samples such as PLA, CNC/PLA, and CNC/rGO/PLA were evaluated using the ISO 22196:2007(E) standard protocol against E. coli (ATCC 25922) and S. aureus (ATCC 25923). The nanocomposites and polyethylene films were sectioned into dimensions of 50x50 and 40x40 mm^2, respectively. PLA samples without rGO loading served as negative controls, while PLA samples with rGO loading served as positive controls. Prior to the experiment, all squares underwent sterilization via autoclaving, while every glass container & instrument was exposed to UV light for a duration of 30 minutes. E. coli and S.aureus, which were cultured on LB and NB agar plates, respectively, the zone of inhibition was examined using the qualitative disc diffusion method. Subsequently, a bacterial suspension with a concentration of $2x10^6$ CFU/mL was applied onto each sample at a volume of 0.4 mL. The samples were then covered with polyethylene film to facilitate the even distribution of the bacterial suspension towards the periphery. Following a 24-hour incubation period at 37°C and 90% relative humidity, the samples and polyethylene films were washed with 10 mL of PBS (phosphate-buffered saline) using gentle shaking for a duration of 1 hour. Subsequently, 0.01 mL of each dilution was aseptically transferred into individual Petri dishes. The procedure for bacterial dispersion involved the careful agitation of 15 mL of plate count agar within separate Petri dishes. The Petri dishes were then incubated at 37°C for a duration of 24 hours and the microbial colony's zone of inhibition was observed.

2.2.8 Contact Angle measurement: The sessile drop method was employed by utilizing KYOWA interface measurement and analysis system to measure the contact angles of distilled water on PLA, CNC/PLA and CNC/rGO/PLA samples . The study involved the measurement of equilibrium contact angles, which were evaluated at a time interval of 60 seconds. The droplet volumes used for the experiment were 6 μL, and measurements were taken in ten distinct locations for each experimental condition. Image J was used to perform the computations necessary to determine the contact angles. Before undergoing analysis, each of the samples that were tested was put through the identical testing procedure and was visually examined to check for imperfections.

2.2.9 In Vitro Lysozyme Degradation Test: The degradation of PLA and its composites was conducted with phosphate buffer saline solution (PBS, pH ~7.4) containing 800 mg/L of lysozyme [35]. In order to expedite the degradation process of the composite and facilitate the timely completion of the study, the concentration of lysozyme was raised from 0.5 mg/ml to 0.8 mg/ml, as previously reported by Novakovic et al. for chitosan-genipin hydrogels [36]. After putting the samples to the vials, the enzyme solution was applied in precise amounts to each sample. The vials were then shaken in an orbital shaker at 35°C and 60 rpm. The process of enzymatic degradation was carried out for a period of four weeks, during which the lysozyme solution was replenished every third day. Samples were collected from the medium at specific intervals of 1, 2, 3, and 4 weeks. These samples were subsequently washed with distilled water and subjected to drying at 60°C in an air oven until a constant mass was achieved. The specimens underwent a pre-degradation weighing process (w_1) and a post-degradation weighing process (w_2) in vitro. The weight loss relative to the starting weight of the sample was used to calculate the deterioration degree (Δw) :

$$\Delta w(\%) = \left(\frac{w_1 - w_2}{w_1}\right) \times 100 \qquad \text{.....(1)}$$

Samples were incubated without lysozyme to be used as a control at the same condition.

3. Results and Discussion:

3.1. Fourier transform infrared spectroscopy (FT-IR)

The presence of the functional groups in the nanocomposites was investigated using FT-IR spectroscopy. Spectra of sample 2 and 3 in fig. 1 provides evidence that nanofillers are present in PLA nanocomposites. The incorporation of CNC in PLA was demonstrated through the presence of characteristic absorption bands. CH_3 stretching band at 2917 cm^{-1} and the CO stretching vibration band at 1659 cm^{-1} can be observed in the infrared spectrum of PLA. Additionally, the broad O-H stretching band of cellulose nanocrystals (CNC) was also detected. The O-H stretching peak observed in the pure PLA material at approximately 3640-3490 cm^{-1} exhibited a slight shift towards the range of 3620-3469 cm^{-1} in the Sample B. The observed displacement of the O-H stretching peak in Sample B nanocomposite is likely attributed to the presence of strong hydrogen bonding interactions between polylactic acid (PLA) and cellulose nanocrystals (CNC), which subsequently weaken the hydrogen bonding within the PLA matrix.The spectral feature observed at a wavenumber of 1623 cm^{-1} is likely assigned to the skeletal vibration of the graphite domains. Sample 5, which is the result of combining PLA, CNC, and 0.75% rGO, exhibited all the characteristic absorbance peaks associated with both CNC and PLA. The distinctive absorbance peaks that are responsible for $–CH_3$ stretching, –C=O stretching, and –C-O stretching were all present in the spectra of the nanocomposite, and there was no formation of a new peak. This phenomenon may be attributed to the absence of functional groups on reduced graphene oxide (rGO), leading to a weak interaction between rGO and the polymer matrix. Consequently, no chemical interaction occurred between rGO and the polylactic acid (PLA) matrix. Therefore, any alterations in the remaining characteristics were solely attributed to the physical interaction between reduced graphene oxide (rGO) and the polylactic acid (PLA) matrix. The spectral analysis validated the existence of CNC in nanocomposite,

signifying that the inclusion of rGO into CNC/PLA nanocomposite did not show any noteworthy effect on the peaks.

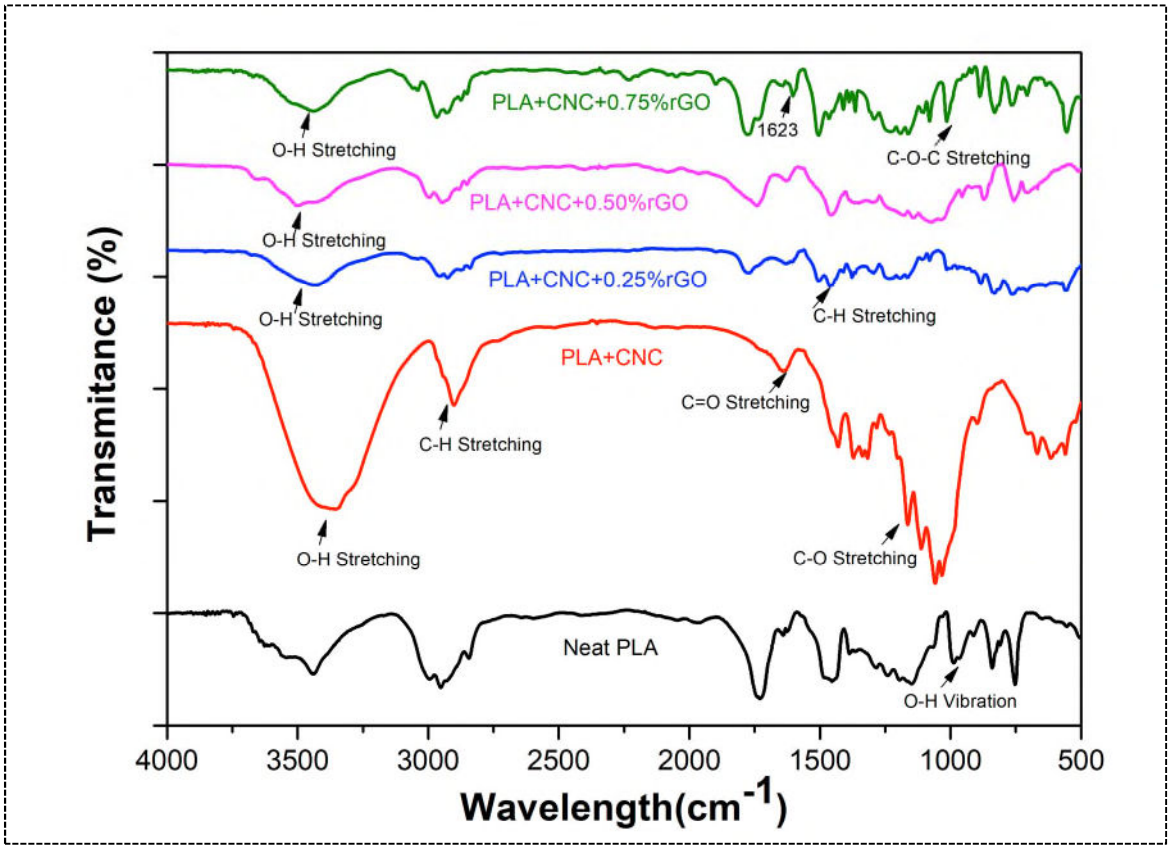

Fig 1: FTIR Spectra for neat PLA, PLA and 1wt% CNC, PLA/CNC/0.25%rGO, PLA/CNC/0.50%rGO, and PLA/CNC/0.75% rGO respectively.

3.2. XRD Analysis:

The polylactic acid sample (PLA) exhibited distinct peaks at 2 θ values of 15, 17, 19° and 23° [37]. The crystalline peaks of PLA were observed to be absent subsequent to the process of extrusion. The observed phenomenon could potentially be attributed to the quenching process, which involves exposure to air atmosphere, during the melting of PLA. Additionally, the rapid cooling rate may have impeded the rearrangement of the crystalline structure. Furthermore, research has demonstrated that PLA derived from natural sources exhibits the least amount of crystallinity when compared to all other types of PLA

nanocomposites. The absence of the distinctive peak observed in rGO powder within the rGO/PLA/CNC nanocomposites is typically indicative of the complete exfoliation of rGO powder within the polymer matrix. It's clear from this that intense shearing during melt-mixing has exceeded the thickness of the collected layers of rGO. The study revealed that the absorption peaks exhibited by the rGO/PLA/CNC nanocomposites were almost indistinguishable from those of the unmodified PLA at all percentage. This indicates that the matrix and the nanofiller don't have any new bonds formed or significant chemical interactions.

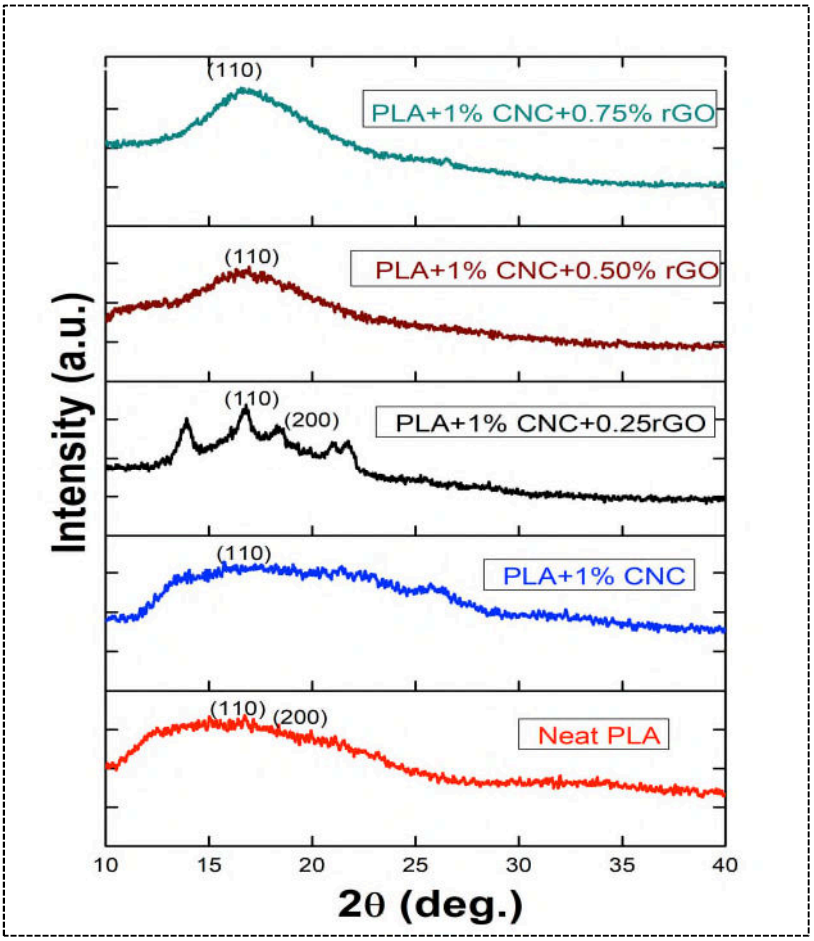

Fig 2: XRD graph for neat PLA (Sample 1), PLA and 1wt% CNC (Sample 2), PLA/CNC/0.25wt% rGO (Sample 3), PLA/CNC/0.50wt% rGO (Sample 4), and PLA/CNC/0.75wt% rGO (Sample 5), respectively.

3.3. FE-SEM :

Results from FE-SEM were utilized to analyze the surface morphology of the fractured sample and to provide a qualitative picture of how the rGO was distributed throughout the PLA/CNC matrix. Micrographs of the composites' surfaces (rGO/PLA/CNC, PLA /CNC, and pristine PLA) are displayed in Figure 3. So as to comprehend the dispersion of rGO in the composite of polylactic acid (PLA) and CNC, it is postulated that the crumpled structure of rGO is imperative for mechanical interlocking with the polymer matrix. It consequently, facilitates the formation of solid interfacial interactions across the interface. The rGO particles are observed to be situated at the interface of the PLA/CNC matrix and are confined within the matrix, resembling a sandwich-like structure in certain regions. This suggests the presence of an electrostatic interaction between the rGO powder & host matrix. The agglomeration of CNC in the matrix, as confirmed by XRD analysis, is depicted in Figure 3(c). A high level of composite uniformity is indicative of a favorable degree of rGO dispersion, which in turn leads to desirable thermal stability. Moreover, it is apparent that the small-sized rGO particles display an inclination to coalesce due to their inherent characteristics. It is widely acknowledged that an appropriate concentration of reduced graphene oxide (rGO) nanoparticles can result in a uniform dispersion within the matrix and mitigate the occurrence of aggregation.

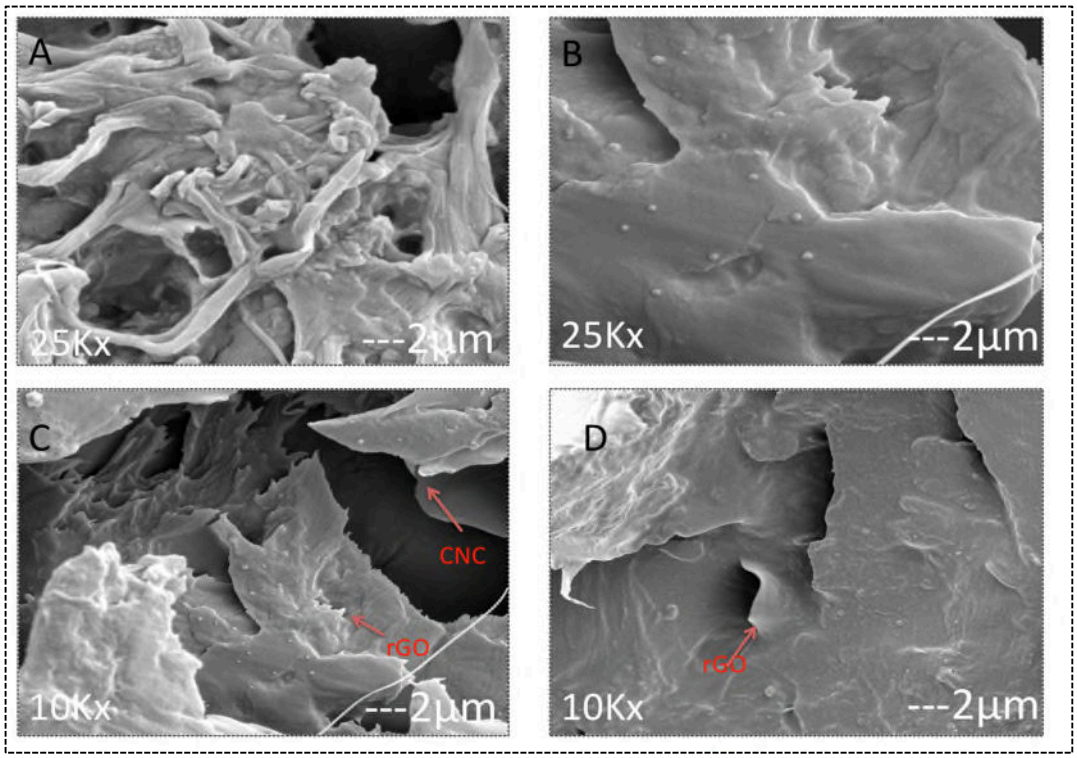

Fig 3: FESEM images for (A) sample 1(neat PLA), (B) sample 2(1% CNC+PLA), (C) sample 4 (0.50%rGO +1% CNC +PLA), and (D) sample 5 (0.75%rGO +1% CNC +PLA), respectively.

3.4. BET Analysis:

The specific surface areas of PLA and PLA-based other composites was obtained using BET surface area analysis, and corresponding BET isotherm is depicted in Figure 4 . The presence of hysteresis loops in the N_2 adsorption/desorption graphs indicates that N_2 gas condenses within the pores by capillary action, confirming the mesoporous character of the samples [38]. The surface area of pure PLA was measured to be 25.82 m^2/g. The surface area of PLA + 1% CNC has been slightly increased to 29.71 m^2/g. After the incorporation of CNC, the surface area of the composite has not been improved as expected and this is mainly due to the blockage of PLA pores in presence of CNC, as evident form the FESEM analysis. Moreover, the total pore volume of PLA (0.031 cc/g) has not been also increased so much after the incorporation of CNC in PLA + 1% CNC composite (0.033 cc/g). However, the surface areas of rGO based PLA + 1% CNC composites have been increased

as compared to bare PLA. The specific surface areas of PLA + 1% CNC + 0.25% rGO, PLA + 1% CNC + 0.50% rGO, and PLA + 1% CNC + 0.75% rGO were found to be 34.04, 40.87, and 46.65 m^2/g, respectively. It is well known that being a 2D material rGO has high surface area. Consequently, the surface areas of composites based on reduced graphene oxide (rGO) have exhibited an increase in comparison to those of pure polylactic acid (PLA). From the FESEM analysis, it is also found that the degree of porosity has been increased for PLA + 1% CNC + 0.25% rGO and PLA + 1% CNC + 0.75% rGO composites in comparision to PLA + 1% CNC. The homogeneous dispersion of PLA and CNC over the rGO sheets is the important cause to increase the porosity as well as surface area. PLA composite material containing 1% CNC and 0.75% rGO exhibited the highest specific surface area, measuring 46.65 m^2/g. In case of PLA + 1% CNC + 0.75% rGO, the total pore volume is also maximum as compared to other samples and it was found to be 0.057 cc/g. Table 2 presents a tabularized summary of thetotal pore volume, specific surface area & pore diameter for all materials. The pore size distribution plots of all samples also imply the mesoporous characteristics (Figure 4 a). The mean pore size of pristine PLA was determined to be 3.134 nm, whereas PLA + 1% CNC + 0.75% rGO composite shows the average pore diameter value of 3.123 nm.

Table 2: Pore volumes, surface areas, and pore diameter of PLA, CNC/PLA and rGO/CNC/PLA samples

	Surface Area (m^2/g)	**Pore Volume (cc/g)**	**Pore diameter (nm)**
Sample 1	25.82	0.031	3.134
Sample 2	29.71	0.033	3.134
Sample 3	34.04	0.038	3.137

Sample 4	40.87	0.049	3.303
Sample 5	46.65	0.057	3.123

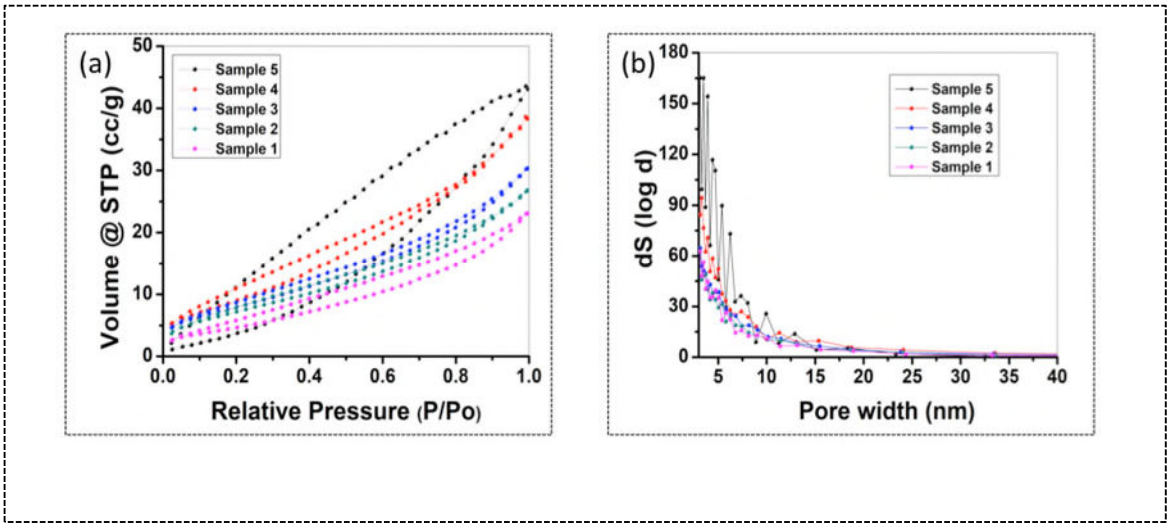

Fig 4: Surface area and pore volume graphs obtained from BET analysis of PLA, CNC/PLA and rGO/CNC/PLA samples.

3.5. Thermogravimetric Analysis (TGA) :

Figure 5 is a thermogram of the thermogravimetric analysis (TGA) curves used to analyze the thermal behavior of rGO/CNC/PLA and CNC/PLA nanocomposites. The temperatures at which their degradation began (T_{onset}), reached their maximum (T_{max}), and reached 90% of their original weight (T_{90}) are all summarized in Table 3. The observed 1% reduction in weight for PLA at temperatures below 200°C may be assigned to the adsorbed water [39]. The PLA polymer degraded at temperature ranges from 300 to 400 °C, which contributed to the second significant weight loss. It is evident from the figure that PLA/CNC composite has better thermal stability than neat PLA and slightly less stability than composites having rGO as nanofiller. Material's better thermal stability may be linked to reduced chain mobility at the rGO interface, resulting from the robust interactions with rGO. The enhancement of thermal stability in nanocomposites was assigned to the barrier effect of rGO's layered structure which impeded the evaporation of chemicals generated during

thermal degradation. When PLA is reinforced with rGO, labile oxygenation groups undergo pyrolysis, which results in the thermochemical degradation of the residual organic content of PLA along with rGO. This weight loss occurred after 400 °C. Over time, the thermal conductivity (T_{onset}), maximum thermal stability (T_{max}), and T_{90} of PLA experienced a gradual rise upon the assimilation of CNC (1%) and rGO nanofillers, as presneted in Table 3. The observed phenomenon could potentially be credited to the synergistic impact of rGO and CNC in the host (PLA) matrix. The study determined that the assimilation of CNC into the host matrix resulted in improved thermal stability. Furthermore, the incorporation of rGO further improved its thermal stability.

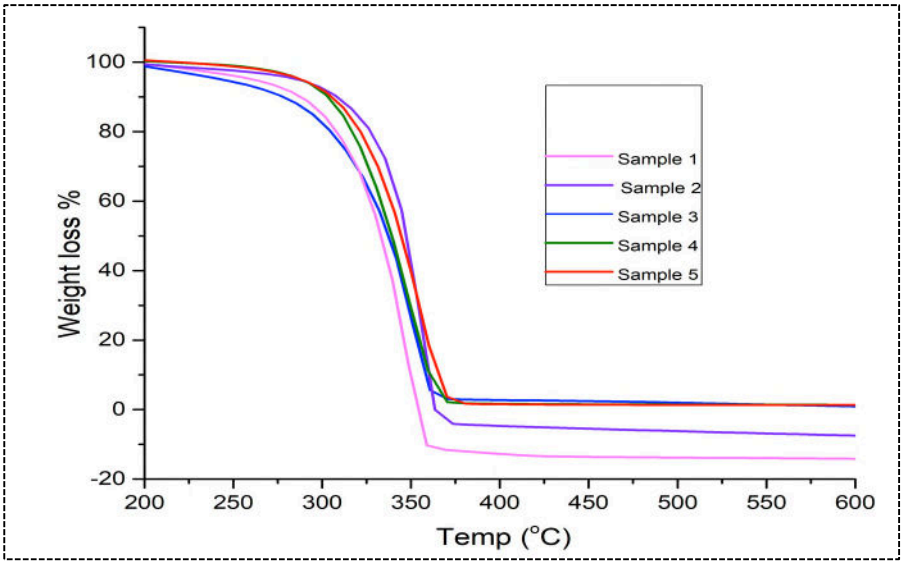

Fig 5: TGA graph of neat PLA (Sample 1), PLA and 1wt% CNC (Sample 2), PLA/CNC/0.25%rGO (Sample 3), PLA/CNC/0.50%rGO (Sample 4), and PLA/CNC/0.75%rGO (Sample 5), respectively.

Table 3: Decomposition Temp of PLA and composites dervied from TGA graph

	T_{onset} (°C)	T_{max} (°C)	T_{90} (°C)
Sample 1	323.6	351.3	363.1
Sample 2	326.2	354.6	366.7
Sample 3	327.9	355.8	369.3

Sample 4	328.5	357.3	371.2
Sample 5	328.9	359.4	374.5

3.6. Differential scanning calorimetry (DSC):

Analyses using differential scanning calorimetry (DSC) were carried out in order to evaluate the effect that adding rGO and CNC had on the crystallinity of polylactic acid (PLA), in addition to the temperature at which it glass transitioned (Tg), the temperature at which it cold crystallized (Tcc), and the temperature at which it melted (Tm). In Table 4, along with the estimated crystallinity, measurements of melting point (T_m), glass transition(T_g) and enthalpy of fusion(ΔH_f), and are summarized. The 1st heating scan was used to examine the as-blown thermal characteristics of the film. The 2nd heating scan, which was performed after the material's thermal history had been cleaned up, was used to analyze the material's intrinsic features. No significant alterations in the Tg of the polylactic acid (PLA) films were detected upon the incorporation of cellulose nanocrystals (CNC) during the initial and subsequent heating scans. The alteration of a material's Tg can be attributed to intermolecular interaction and chain flexibility. Conversely, melting point (Tm) values and area under the curve (enthalpy of fusion(ΔH_f) values increased with increasing rGO wt%. The findings suggest that the incorporation of blends of rGO and CNC has the potential to influence the thermal characteristics of PLA. As anticipated, the introduction of a small quantity of CNCs did not produce a substantial alteration in the chain flexibility or intermolecular interaction of PLA, and thus did not result in a significant impact on its Tg [40]. The Tc values observed in the initial and subsequent heating scans of PLA/CNC/rGO films were notably lower than those of the control films consisting of neat PLA. The above observation implies that the speeding up the crystallization process

can be linked to the nucleation effect of CNCs, which is consistent with the fundamental principles of heterogeneous nucleation theory [41].

In summary, the outcomes of this research indicate that the incorporation of blends comprising rGO and CNC can modify the thermal characteristics of PLA. This could potentially have significant ramifications for the utilization of PLA in diverse applications. The enhancement of thermal properties of PLA matrix can be achieved through an increase in its thermal conductivity & degree of crystallinity. Because of this improvement, it can be used in a wider variety of high-performance contexts, such as packaging, biomedical implants, and cutting-edge materials. Additional investigation is required to comprehensively comprehend the impression of rGO and CNC amalgamations on the thermal characteristics of PLA and to enhance their applicability in diverse contexts.

Table 4: DSC analysis of PLA, CNC/PLA and CNC/rGO/PLA nanocomposites.

	T_g (°C)	T_{cc}(°C)	T_m(°C)	ΔH_f(J/g)	χ (%)
Sample 1	65.32	119.24	151.37	18.05	14
Sample 2	62.45	118.37	152.88	18.10	15
Sample 3	59.28	121.32	153.20	19.24	17
Sample 4	57.54	117.67	154.34	22.48	20
Sample 5	56.82	114.83	163.70	27.50	26

Tg - glass transition Temp, T_{CC}- cold crystallization Temp, Tm- melting Temp ΔH_f – enthalpy of fusion, χ- crystallinity

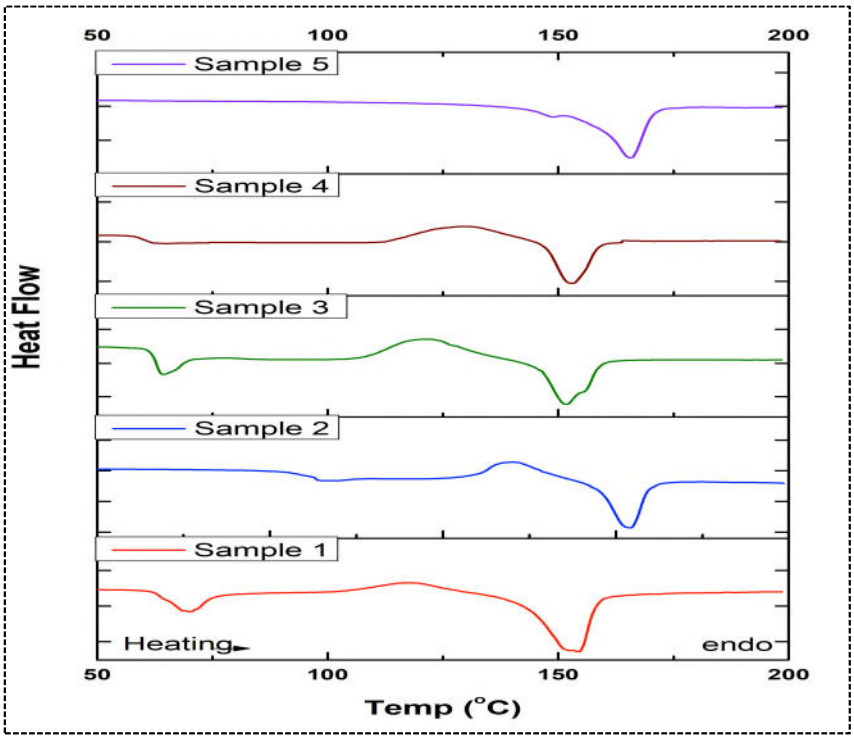

Fig 6: DSC graphs showing Tg, Tm and Tcc of PLA, CNC/PLA and CNC/rGO/PLA nanocomposites.

3.7. In Vitro Biodegradation Test:

The assessment of the enzyme-mediated degradation of biomedical scaffolds is commonly conducted through the measurement of the reduction in weight. The present investigation involved subjecting PLA, CNC/PLA, and CNC/rGO/PLA composites to a formal in vitro degradation study. This was achieved by immersing the aforementioned materials in Lysozyme chloride buffer for a duration of 28 days. Based on the findings depicted in the figure 7, it is evident that the pure PLA material exhibits a comparatively lower rate of degradation in contrast to the CNC/PLA and CNC/rGO/PLA composites. The degradation rates of PLA and CNC/PLA and CNC/0.75% rGO/PLA were assessed to be 5.6±0.3% and 9.8±0.1%, respectively, following a 28-day immersion in Lysozyme chloride. The assimilation of CNC into the host matrix (PLA) results in a notable enhancement of the degradation process of PLA. In contrast to the research conducted by Belaid et al. regarding

the 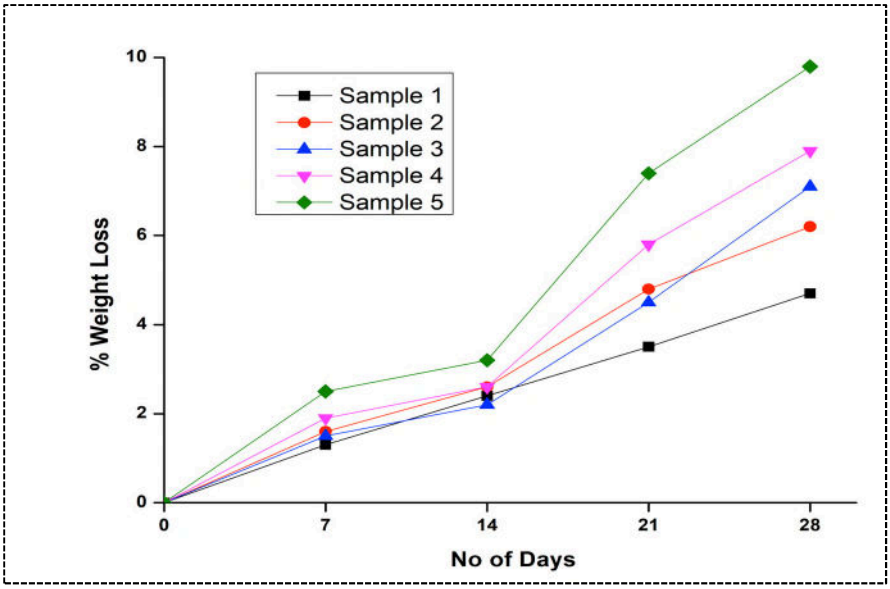

utilization of PLA and graphene oxide (PLA/GO) composite scafolds, the assimilation of CNCs results in a moderate enrichment of the degradation rate of PLA scafolds when exposed to alcalase [42]. Therefore, CNC seems to be an appropriate choice for PLA's reinforcing. Hence, it is plausible to consider CNC/rGO/PLA biocomposite as a viable material for the fabrication of scaffolds, which can serve as a temporary replacements, particularly for the purpose of bone tissue regeneration [43].

Fig 7: Time-dependent degradation study of PLA, CNC/PLA and CNC/rGO/PLA nanocomposites

3.8 Contact angle Measurement and Wettability

Hydrophilicity looks critical for scafold performance in any application of tissue engineering, including bone regeneration, because it significantly affects cell proliferation adhesion and rehydration capability. Thus, the contact angle could be used as a predictor of the scafolds' reactivity and interaction with the surrounding surface. Because of its rearranged state in the PLA matrix, CNC imparts a hydrophilic feature to the hydrophobic surface of PLA scafolds. The pure PLA material exhibits hydrophobic characteristics, as evidenced by a contact angle measurement of 100^0. Contact angle observations from the scafolds indicate that the incorporation of CNC increases PLA's ability to absorb water. Murphy et al. reported comparable outcomes in terms of water retention for PLA and PLA/cellulose filaments [44]. The results indicate that the water contact angles of PLA/CNC/rGO scaffolds were comparatively lower than those of PLA scaffolds, as illustrated in Figure 8. Pinto et al. have documented analogous findings pertaining to the impact of graphene oxide (GO) incorporation on polylactic acid (PLA) films and observed a reduction in the contact angle of approximately 9° upon the addition of GO [6]. The aforementioned observation implies that the hydrophilicity of the scaffold surface is improved by the presence of GO, and that the surface characteristics of the final material are directly influenced by the employed methodology. The result shows that the initial contact angle of pure PLA was measured to be 100°, whereas the contact angle of PLA containing 0.75% rGO was found to be 69°. It's possible that the liquids' direct interactions with the PLA surface's partially exposed fillers are responsible for this reduction. The elucidation of the behavior into account can be attributed to the hydrogen bond interactions that take place between the oxygen-containing groups present in reduced graphene oxide

(rGO) and water. In conclusion, including rGO and CNC into the host matrix (PLA) reduced the surface hydrophobic characteristics, which should promote better cell adhesion and proliferation.

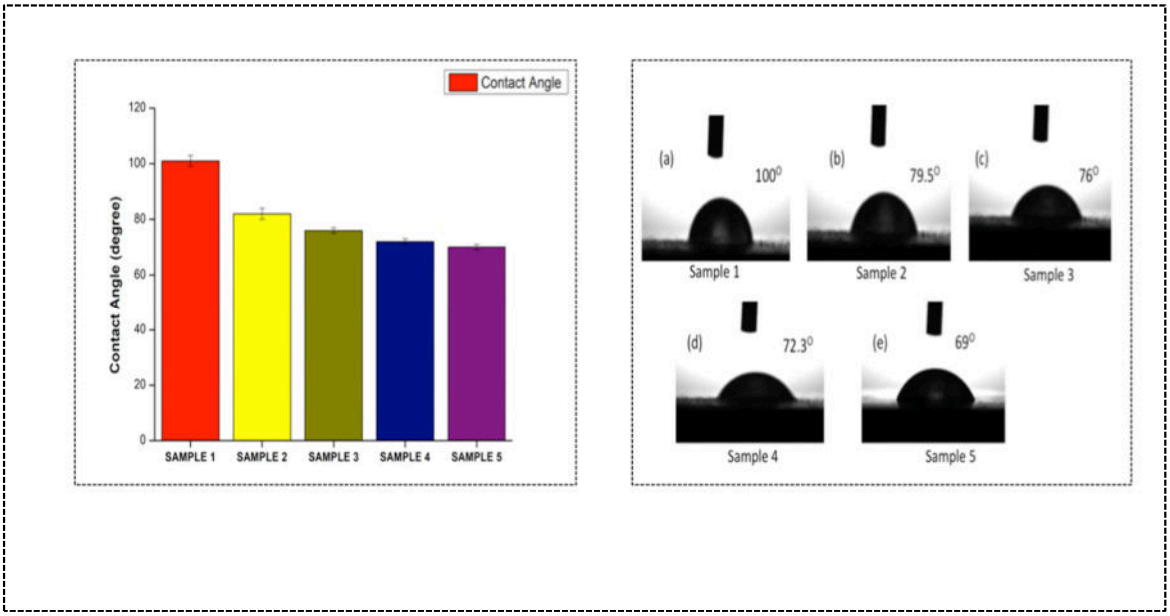

Fig 8 : Contact Angle measurement of different PLA based nanocomposites.

3.9 Antibacterial Assesment:

The agar disc diffusion process is widely regarded as a primary technique for assessing the bioactive characteristics in food packaging application [31]. This is due to its ability to function as a quantitative assay and replicate the conditions of food storage. Both S.aureus (Gram-positive) and E. coli (Gram-negative) were implied to test the antibacterial efficacy of PLA and its nanocomposite. The study conducted a qualitative disc diffusion assay and observed that sample 3 and sample 4 exhibited superior antibacterial efficacy in comparison to sample 2. The enhanced hydrophilic properties of the composites result in the formation of a surface that inhibits the growth of bacteria. This effect is further strengthened by the amphiphilic nature of the surface. The influence of composite roughness on antimicrobial efficacy warrants further investigation, as bacterial adhesion has been shown to be sensitive

to this parameter. The lower antibacterial performance observed in sample 2 may be attributed to this factor, which is supported by the findings of the BET analysis. The results indicate that the antibacterial efficacy of nanocomposites shows somewhat higher effect on S.aureus compared to E. coli, as illustrated in Figure 9.

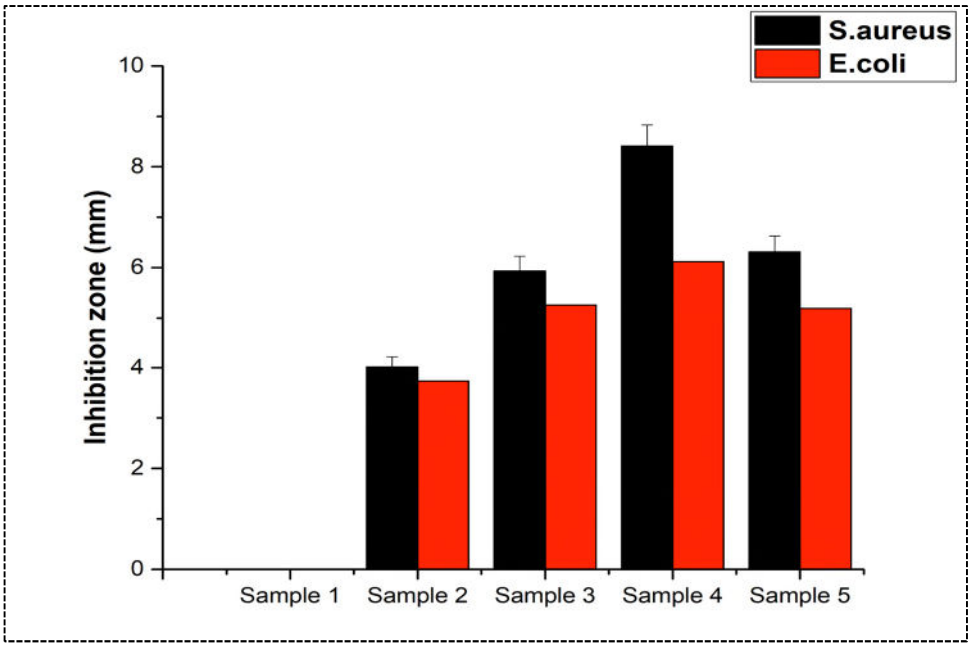

Fig 9: Antibacterial assessment for PLA ,CNC/PLA and CNC/rGO/PLA nanocomposites against S. aureus and E. coli bacteria.

Table 5 : Antibacterial evaluation of different PLA based nanocomposites against S. aureus and E. coli

	Inhibition Zone Diameter (mm)	
	S. aureus	**E. coli**
Sample 1	-	-
Sample 2	4.01± 0.14	3.73± 0.09
Sample 3	5.93± 0.16	5.26± 0.21
Sample 4	8.41± 0.31	6.12± 0.43
Sample 5	6.31± 0.20	5.19± 0.15

4. Conclusion:

The present research resulted in the synthesis of composites consisting of PLA reinforced with rGO/CNC as well as a thorough assessment of those composites by carried out few characterization technique. The focus of the investigation was primarily on the structural, morphological & thermal characterization of the composites, along with their biocompatibility. The work reports the successful incorporation of rGO and CNC as nanofillers in host matrix (PLA) via melt mixing. The nanocomposite exhibited a well-controlled morphology. overall, our experimental findings indicate that the utilization of reduced graphene oxide (rGO) resulted in an augmentation of surface roughness and hydrophilicity. Additionally, an enhancement in crystallinity was found. No discernible change in Tg was brought due to the addition of Nanofiller (rGO). However, it contributed to an enhancement in the thermal properties of the composite material. The study's findings suggest that the incorporation of CNC and rGO using the melt-mixing process exhibits potential for extensive implementation across diverse industrial sectors. The biodegradation through Lysozyme, contact angle measurement and antibacterial assesment indicate significant potential for the use of these scaffolds in tissue engineering and packaging applications.

Declaration of conflict of interest:

The authors declare that they do not have any conflict of interest.

Acknowledgement:

Authors would like to thank Prof. G.C. Nayak from IIT (ISM) Dhanbad for providing melt mixing facility to carryout this work.

References:

1- Xue W, Du J, Li Q, Wang Y, Lu Y, Fan J, Yu S, Yang Y. Preparation, Properties, and Application of Graphene-Based Materials in Tissue Engineering Scaffolds. Tissue Eng Part B Rev. 2022 Oct;28(5):1121-1136. doi: 10.1089/ten.TEB.2021.0127

2- Madhavan Nampoothiri K, Nair NR, John RP. An overview of the recent developments in polylactide (PLA) research. Bioresour Technol. 2010 Nov;101(22):8493-501. doi: 10.1016/j.biortech.2010.05.092.

3- Chen BQ, Kankala RK, Chen AZ, Yang DZ, Cheng XX, Jiang NN, Zhu K, Wang SB. Investigation of silk fibroin nanoparticle-decorated poly(l-lactic acid) composite scaffolds for osteoblast growth and differentiation. Int J Nanomedicine. 2017 Mar 8;12:1877-1890. doi: 10.2147/IJN.S129526.

4- Lasprilla AJ, Martinez GA, Lunelli BH, Jardini AL, Filho RM. Poly-lactic acid synthesis for application in biomedical devices - a review. Biotechnol Adv. 2012 Jan-Feb;30(1):321-8. doi: 10.1016/j.biotechadv.2011.06.019.

5- Thakur, Sourbh & Chaudhary, Jyoti & Sharma, Bhawna & Verma, Ankit & Tamulevičius, Sigitas & Thakur, Vijay Kumar. (2018). Sustainability of Bioplastics: Opportunities and Challenges. Current Opinion in Green and Sustainable Chemistry. 13. 10.1016/j.cogsc.2018.04.013.

6- Moreira Pinto, Artur & Cabral, Joana & Tanaka, David & Mendes, Adélio & Magalhães, Fernão. (2013). Effect of incorporation of graphene oxide and graphene nanoplatelets on mechanical and gas permeability properties of poly(lactic acid) films. Polymer International. 62. 10.1002/pi.4290.

7- Jia, Zhaojun & Xu, Xiaoxue & Zhu, Donghui & Zheng, Yufeng. (2023). Design, Printing, and Engineering of Regenerative Biomaterials for Personalized Bone Healthcare. Progress in Materials Science. 134. 101072. 10.1016/j.pmatsci.2023.101072.

8- Oksman K, Mathew AP, Bondeson D, Kvien I. Manufacturing process of cellulose whiskers/polylactic acid nanocomposites. Compos Sci Technol. 2006;66(15):2776-2784. https://doi.org/10.1016/j.compscitech.2006.03.002

9- Trache, Djalal & Hussin, Mohd Hazwan & Haafiz, M.K & Thakur, Vijay Kumar. (2017). Recent progress in cellulose nanocrystals: Sources and production. Nanoscale. 9. 10.1039/C6NR09494E.

10- Ates B, Koytepe S, Ulu A, Gurses C, Thakur VK. Chemistry, Structures, and Advanced Applications of Nanocomposites from Biorenewable Resources. Chem Rev. 2020 Sep 9;120(17):9304-9362. doi: 10.1021/acs.chemrev.9b00553.

11- Raghvendra Kumar Mishra, Sung Kyu Ha, Kartikey Verma, Santosh K. Tiwari, Recent progress in selected bio-nanomaterials and their engineering applications: An overview, Journal of Science: Advanced Materials and Devices, Volume 3, Issue 3,2018, https://doi.org/10.1016/j.jsamd.2018.05.003.

12- Rana AK, Frollini E, Thakur VK. Cellulose nanocrystals: Pretreatments, preparation strategies, and surface functionalization. Int J Biol Macromol. 2021 Jul 1;182:1554-1581. doi: 10.1016/j.ijbiomac.2021.05.119.

13- P. Zhang, D. Gao, P. Zou, B. Wang, Preparation and thermomechanical properties of nanocrystalline cellulose reinforced poly(lactic acid) nanocomposites, J. Appl. Polym. Sci. 134 (2017), https://doi.org/10.1002/app.44683.

14- A.L. Goffin, J.M. Raquez, E. Duquesne, G. Siqueira, Y. Habibi, A. Dufresne, P. Dubois, From interfacial ring-opening polymerization to melt processing of cellulose nanowhisker-filled polylactide-based nanocomposites, Biomacromolecules 12 (2011) 2456–2465, https://doi.org/10.1021/bm200581h.

15- S.S. Borkotoky, P. Dhar, V. Katiyar, Biodegradable poly (lactic acid)/cellulose nanocrystals (CNCs) composite microcellular foam: effect of nanofillers on foam cellular morphology, thermal and wettability behavior, Int. J. Biol. Macromol. 106 (2018) 433–446, https://doi.org/10.1016/j.ijbiomac.2017.08.036

16- Trache D, Thakur VK, Boukherroub R. Cellulose Nanocrystals/Graphene Hybrids-A Promising New Class of Materials for Advanced Applications. Nanomaterials (Basel). 2020 Aug 4;10(8):1523. doi: 10.3390/nano10081523.

17- Maity Chandan , Hatui Goutam , Tiwari Santosh, Udayabhanu, G., Pathak Devendra Deo & Nayak Ganesh & Verma Kartikey. (2019). One pot solvothermal synthesis of novel solid state N-Doped TiO2/n-Gr for efficient energy storage devices. Vacuum. 164. 10.1016/j.vacuum.2019.02.002.

18- A. Kumar, V. Navakoteswara Rao, A. Kumar, M. Venkatakrishnan Shankar, V. Krishnan, ChemPhotoChem 2020, 4, 427.

19- Ashish Bahuguna, Suneel Kumar, Vipul Sharma, Kumbam Lingeshwar Reddy, Kaustava Bhattacharyya, P. C. Ravikumar, and Venkata Krishnan ACS Sustainable Chemistry & Engineering 2017 5 (10), 8551-8567 DOI: 10.1021/acssuschemeng.7b00648

20- Maity, Chandan & Hatui, Goutam & Verma, Kartikey & Udayabhanu, G. & Pathak, Devendra Deo & Nayak, Ganesh. (2018). Single pot fabrication of N doped reduced GO (N-rGO) /ZnO-CuO nanocomposite as an efficient electrode material for supercapacitor application. Vacuum. 157. 10.1016/j.vacuum.2018.08.019.

21- R.B. Valapa, G. Pugazhenthi, V. Katiyar, Effect of graphene content on the properties of poly(lactic acid) nanocomposites, RSC Adv. 5 (2015) 28410–28423, https://doi.org/10.1039/C4RA15669B.

22- Pinto AM, Moreira S, Gonçalves IC, Gama FM, Mendes AM, Magalhães FD. Biocompatibility of poly(lactic acid) with incorporated graphene-based materials. Colloids Surf B Biointerfaces. 2013 Apr 1;104:229-38. doi: 10.1016/j.colsurfb.2012.12.006.

23- Kovaleva, Polina & Pariy, Igor & Chernozem, Roman & Zadorozhnyy, Mikhail & Permyakova, Elizaveta & Kolesnikov, E. & Surmeneva, M. & Surmenev, Roman & Senatov, Fedor. (2022). Shape memory effect in hybrid polylactide-based polymer scaffolds functionalized with reduced graphene oxide for tissue engineering. European Polymer Journal. 181. 111694. 10.1016/j.eurpolymj.2022.111694.

24- Maity, Chandan & Hatui, Goutam & Sahoo, Sumanta & Saren, Pupulata & Nayak, G.. (2019). Boron Nitride based Ternary Nanocomposites with Different Carbonaceous Materials Decorated by Polyaniline for Supercapacitor Application. ChemistrySelect. 4. 3672-3680. 10.1002/slct.201803560.

25- Rajesh Kumar, Sumanta Sahoo, Ednan Joanni, Rajesh K. Singh, Keiichiro Maegawa, Wai Kian Tan, Go Kawamura, Kamal K. Kar, Atsunori Matsuda, Heteroatom doped graphene engineering for energy storage and conversion, Materials Today, 39, 2020, Pages 47-65, https://doi.org/10.1016/j.mattod.2020.04.010.

26- Rajesh Kumar, Sumanta Sahoo, Ednan Joanni, Rajesh Kumar Singh, Wai Kian Tan, Kamal Krishna Kar, Atsunori Matsuda,Recent progress in the synthesis of graphene and derived materials for next generation electrodes of high performance lithium ion batteries,Progress in Energy and Combustion Science, Volume 75,2019,100786,https://doi.org/10.1016/j.pecs.2019.100786.

27- Kumar, Suneel & N., Lakshmana Reddy & Kushwaha, Himmat & Kumar, Ashish & Muthukonda Venkatakrishnan, Shankar & Bhattacharyya, Kaustava & Halder, Aditi & Krishnan, Venkata. (2017). Efficient Electron Transfer across a ZnO–

MoS_2–Reduced Graphene Oxide Heterojunction for Enhanced Sunlight- Driven Photocatalytic Hydrogen Evolution. ChemSusChem. 10. 3588-3603. 10.1002/cssc.201701024.

28- Fei F, Yao H, Wang Y, Wei J. Graphene Oxide/RhPTH(1-34)/Polylactide Composite Nanofibrous Scaffold for Bone Tissue Engineering. Int J Mol Sci. 2023 Mar 18;24(6):5799. doi: 10.3390/ijms24065799.

29- Kumar, Ashish & Kumar, Suneel & Bahuguna, Ashish & Kumar, Ajay & Sharma, Vipul & Krishnan, Venkata. (2017). Recyclable, Bifunctional Composites of Perovskite Type N-CaTiO3 and Reduced Graphene Oxide as an Efficient Adsorptive Photocatalyst for Environmental Remediation. Mater. Chem. Front.. 10.1039/C7QM00362E.

30- Wang D, Lu X, Qu J. Role of in situ thermal-reduced graphene oxide on the morphology and properties of biodegradable poly (lactic acid)/poly (butylene succinate) blends. Polym Compos. 2018;39(9):3057-3065. https://doi.org/10.1002/pc.24310

31- Quintavalla, S. & Vicini, L. (2002). Antimicrobial food packaging in meat industry. Meat Science, 62, 373–380.

32- Liu, Yuzhu & Matuana, Laurent. Surface texture and barrier performance of poly(lactic acid)-cellulose nanocrystal extruded-cast films. Journal of Applied Polymer Science. 136 (2019) 47594

33- Cranston ED, Gray DG. Morphological and optical characterization of polyelectrolyte multilayers incorporating nanocrystalline cellulose. Biomacromolecules. 2006 Sep;7(9):2522-30. doi: 10.1021/bm0602886

34- Tiwari, Santosh & Verma, Kartikey & Saren, Pupulata & Oraon, Ramesh & De Adhikari, Amrita & Nayak, G. & Kumar, Vijay. Manipulating selective dispersion of reduced graphene oxide in polycarbonate/nylon 66 blend nanocomposites for improved thermomechanical properties. RSC Advances. 7(2017). 10.1039/C7RA02044A.

35- Andrea Lončarević, Marica Ivanković, Anamarija Rogina Lysozyme-Induced Degradation of Chitosan: The Characterisation of Degraded Chitosan Scaffolds. Journal of Tissue Repair and Regeneration 1(1) (2017):12-22. https://doi.org/10.14302/issn.2640-6403.jtrr-17-1840

36- Reay, S.L.; Jackson, E.L.; Ferreira-Duarte, A.M.; Hilkens, C.M.U.; Novakovic, K. In vitro evaluation of the biodegradability of chitosan–genipin hydrogels. Mater. Adv. 2022, 3, 7946–7959.

37- Campos, João & Ferraria, Ana & Rego, Ana Maria & Ribeiro, Maria & Barros-Timmons, Ana. (2015). Studies on PLA grafting onto graphene oxide and its effect on the ensuing composite films. Materials Chemistry and Physics. 166. 10.1016/j.matchemphys.2015.09.036.

38- Maity, C.K., Sahoo, S., Verma, K., Behera, A.K. and Nayak, G.C., 2020. Facile functionalization of boron nitride (BN) for the development of high-performance asymmetric supercapacitors. New Journal of Chemistry, 44(19), pp.8106-8119.

39- Villar-Rodil, Silvia & Paredes, Juan & Martínez-Alonso, Amelia & Tascón, Juan. (2009). Preparation of graphene dispersion and graphene–polymer composites in organic media. Journal of Materials Chemistry - J MATER CHEM. 19. 10.1039/b904935e.

40- Liao, Ken-Hsuan & Aoyama, Shigeru & Abdala, Ahmed & Macosko, Christopher. (2014). Does Graphene Change Tg of Nanocomposites?. Macromolecules. 47. 8311-8319. 10.1021/ma501799z.

41- E. Piorkowska and G.C. Rutledge, Handbook of Polymer Crystallization, John Wiley & Sons Publication, New Jersey, pp. 125–163 (2013) ISBN: 978-0-470-38023-9

42- Belaid H, Nagarajan S, Teyssier C, Barou C, Barés J, Balme S, Garay H, Huon V, Cornu D, Cavaillès V, Bechelany M. Development of new biocompatible 3D printed graphene oxide-based scaffolds. Mater Sci Eng C Mater Biol Appl. 2020 May;110:110595. doi: 10.1016/j.msec.2019.110595.

43- Lai, Yen-Han & Chen, Yung-Hsin & Pal, Arnab & Chou, Syun-Hong & Chang, Shwu-Jen & Huang, E-Wen & Lin, Zong-Hong & Chen, San-Yuan. (2021). Regulation of Cell Differentiation via Synergistic Self-powered Stimulation and Degradation Behavior of a Biodegradable Composite Piezoelectric Scaffold for Cartilage tissue. Nano Energy. 90. 106545. 10.1016/j.nanoen.2021.106545.

44- Murphy, Caroline & Collins, Maurice. (2016). Microcrystalline cellulose reinforced polylactic acid biocomposite filaments for 3D printing. Polymer Composites. 39. 10.1002/pc.24069.

Development of reduced graphene oxide (rGO) reinforced poly(lactic) acid/ cellulose nanocrystal composite through melt mixing: Effect of nanofiller on thermal, structural, biodegradation and antibacterial properties

Verma, Kartikey

2023-08-26

Verma K, Siddiki SH, Maity CK,et al., (2023) Development of reduced graphene oxide (rGO) reinforced poly(lactic) acid/ cellulose nanocrystal composite through melt mixing: effect of nanofiller on thermal, structural, biodegradation and antibacterial properties. Industrial Crops and Products, Volume 204, Part B, Article number 117307.

https://doi.org/10.1016/j.indcrop.2023.117307